Supporting Information

In Situ Metal Organic Framework (ZIF-8) and Mechanofusion-Assisted MWCNT Coating of $LiFePO_4$/C Composite Material for Lithium-Ion Batteries

Priyatrisha Mathur[a,b], Jeng-Ywan Shih[b], Ying-Jeng James Li[a,b], Tai-Feng Hung[a], Balamurugan Thirumalraj[c], Sayee Kannan Ramaraj[d], Rajan Jose[e], Chelladurai Karuppiah[a,*], Chun-Chen Yang[a,b,f*]

[a]Battery Research Center of Green Energy, Ming Chi University of Technology, New Taipei City 24301, Taiwan, ROC.

[b]Department of Chemical Engineering, Ming Chi University of Technology, New Taipei City 24301, Taiwan, ROC.

[c]School of Materials Science & Engineering, Kookmin University, Seoul 02707, Republic of Korea

[d]PG and Research Department of Chemistry, Thiagarajar College, Madurai, Tamil Nadu, India.

[e]Nanostructured Renewable Energy Materials Laboratory, Faculty of Industrial Sciences and Technology, University Malaysia Pahang, 26300 Kuantan, Malaysia.

[f]Department of Chemical and Materials Engineering, Chang Gung University, Kwei-shan, Taoyuan 333, Taiwan, R.O.C.

***Corresponding authors:** kcdurai.rmd@gmail.com (C.K); ccyang@mail.mcut.edu.tw (C.-C.Y); **Tel.:** +886-2-29089899 (ext.4962/4952) (C.K.); **Fax:** +886-2-29085941 (C.K.)

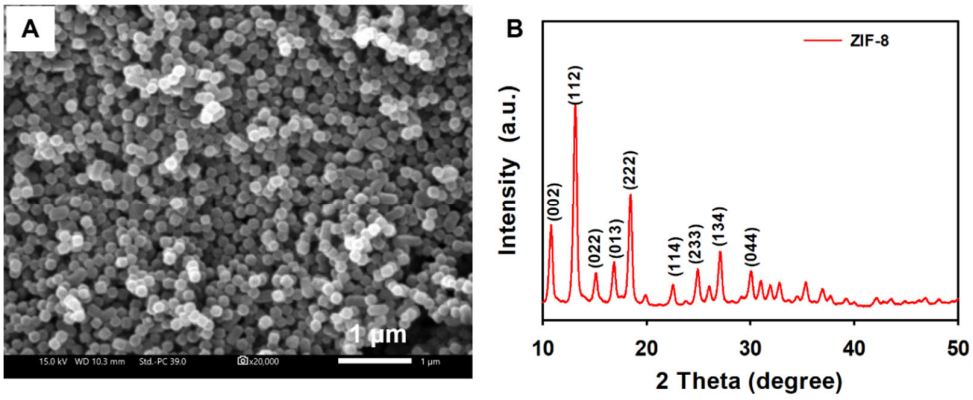

Figure S1. (A) SEM image of the pristine ZIF-8 nanoparticle. (B) XRD pattern of the pristine ZIF-8 nanoparticle.

In this study, the deposition of ZIF-8 on LFP was followed by adding different dosage of reactants not controlling the deposition time. As reported earlier [25], the yield percentage of ZIF-8 was about roughly 25% of the total amount of zinc nitrate hexahydrate used. This information was used to calculate the amount of zinc nitrate hexahydrate to be used to obtain the desired weight percentage of ZIF-8 that would be deposited on LFP. Here also, the zinc nitrate hexahydrate and 2-methylimidazole were mixed in the molar ratio of 1:8. Thus, by varying the zinc nitrate hexahydrate amount and maintaining the above 1:8 ratio, different wt.% depositions of ZIF-8@LFP was obtained. Surface modification of LiFePO4 by various percentage compositions of ZIF-8 are given below in **Table S1**.

Table S1. Different formulation of ZIF-8 deposition on LFP materials

Sample	ZIF-8 content (wt.%)	Materials			
		Zinc nitrate hexahydrate (mmol)	2-methylimidazole (mmol)	LFP (g)	Ethanol (mL)
1 wt.% ZIF-8@LFP	1	0.44	3.51	5	70
2 wt.% ZIF-8@LFP	2	0.88	7.03		
3 wt.% ZIF-8@LFP	3	1.32	10.54		

4 wt.% ZIF-8@LFP	4	1.76	14.06

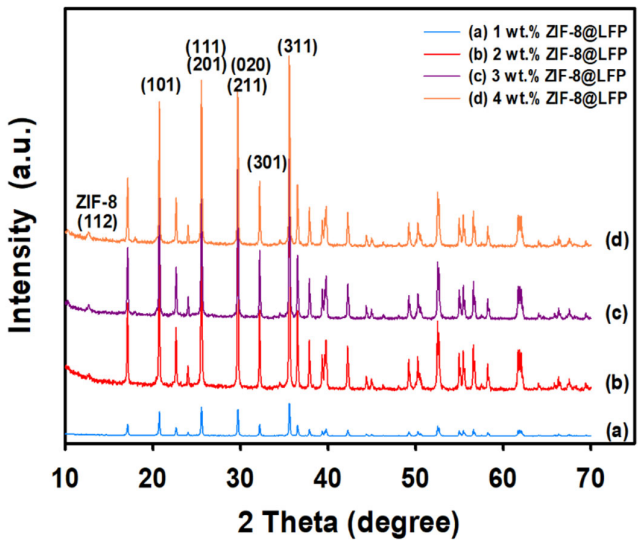

Figure S2. XRD patterns of the (a) 1 wt.% ZIF-8@LFP, (b) 2 wt.% ZIF-8@LFP, (c) 3 wt.% ZIF-8@LFP and (d) 4 wt.% ZIF-8@LFP composites, which were prepared by a magnetic stirring method.

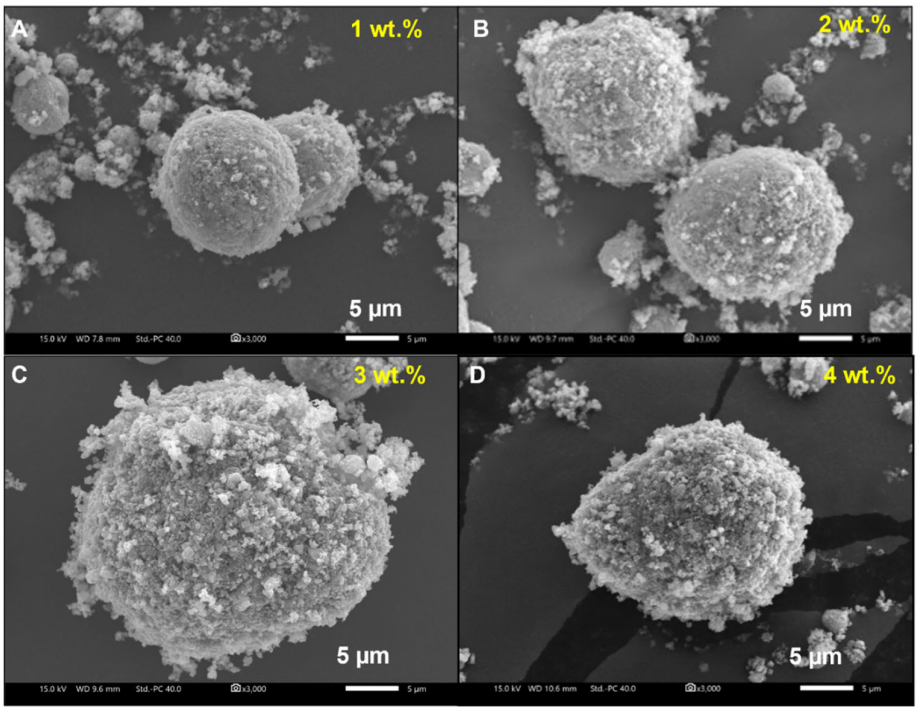

Figure S3. SEM images of the **(A)** 1 wt.% ZIF-8@LFP, **(B)** 2 wt.% ZIF-8@LFP, **(C)** 3 wt.% ZIF-8@LFP and **(D)** 4 wt.% ZIF-8@LFP composites, which were prepared by a magnetic stirring method.

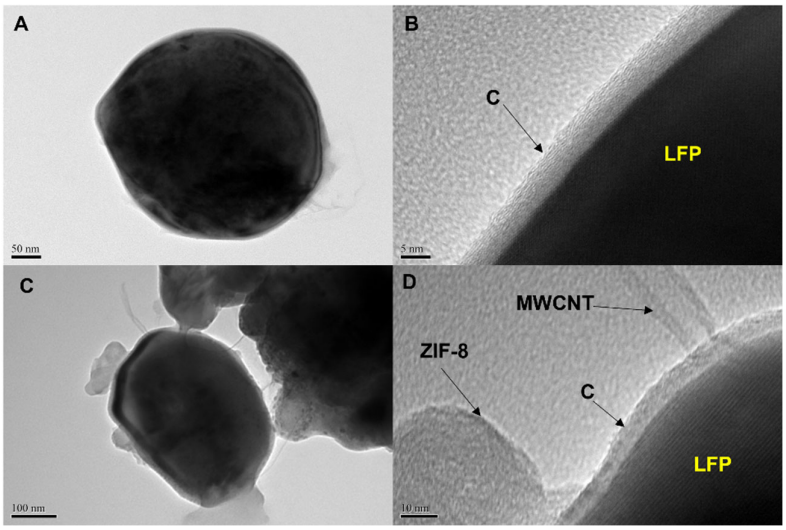

Figure S4. (A,B) TEM images of the bare LFP. **(C,B)** 2 wt.% ZIF-8@LFP [A]/MWCNT composite.

Table S2. Comparative analysis of the intensity ratio (I_D/I_G) of the different LFP composite materials.

Sample	I_D	I_G	I_D/I_G
bare LFP	4281.13	5075.96	0.8434
2 wt.% ZIF-8@LFP [A]	4527.52	5198.79	0.8709
2 wt.% ZIF-8@LFP [A]/MWCNT	3741.93	4337.77	0.8626

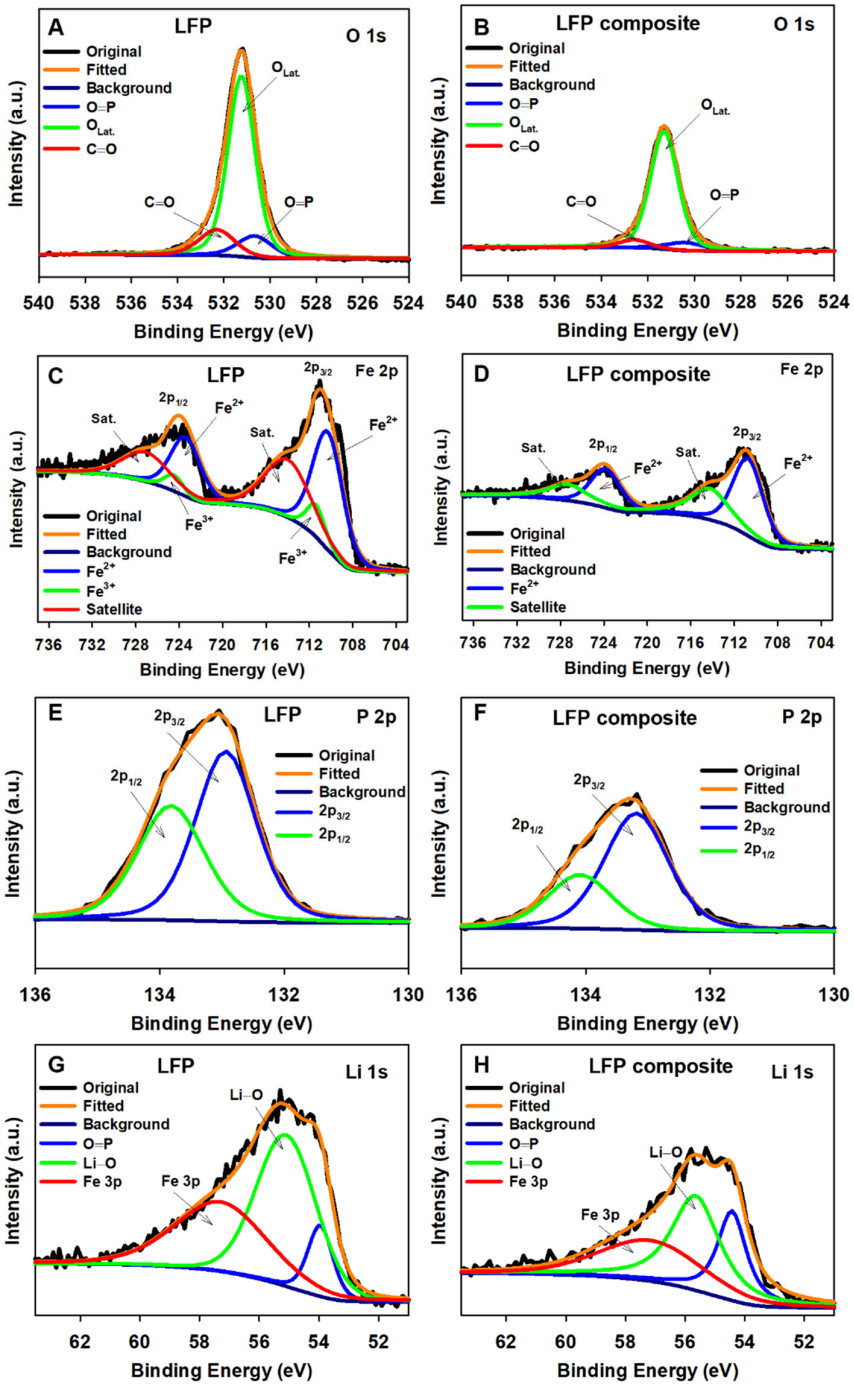

Figure S5. XPS deconvolution spectra of (A,B) O 1s, (C,D) Fe 2p, (E,F) P 2p and (G,H) Li 1s peaks of the bare LFP and LFP composite (2% ZIF-8@LFP [A]/MWCNT).

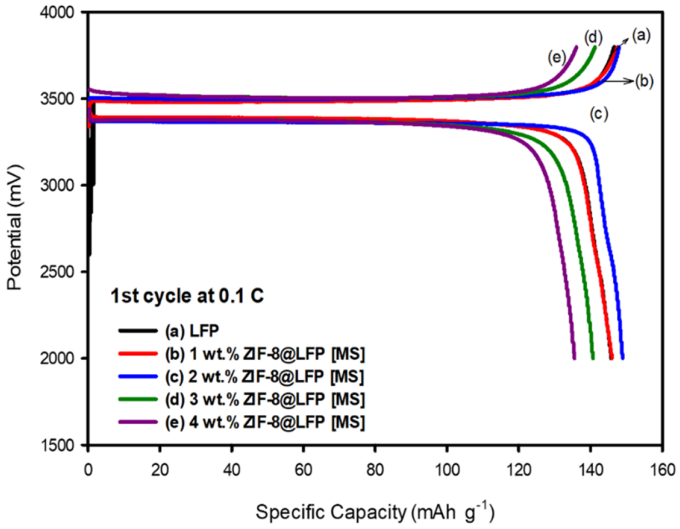

Figure S6. First charge-discharge profile for the (a) bare LFP, (b) 1 wt.% ZIF-8@LFP [MS], (c) 2 wt.% ZIF-8@LFP [MS], (d) 3 wt.% ZIF-8@LFP [MS], and (e) 4 wt.% ZIF-8@LFP [MS] electrodes.

Table S3. Comparative electrochemical performance results for different ZIF-8@LFP formulations.

Sample	Specific capacity Q_{sp} (mAh g^{-1})		CE%
	Q_{sp}_Charge	Q_{sp}_Discharge	Q_{sp}_Dis/Q_{sp}_Ch
bare LFP	144.57	143.06	98.95
1 wt.% ZIF-8@LFP [MS]	146.54	144.95	98.92
2 wt.% ZIF-8@LFP [MS]	146.57	145.69	99.39
3 wt.% ZIF-8@LFP [MS]	142.85	141.54	99.00
4 wt.% ZIF-8@LFP [MS]	136.07	135.53	99.05

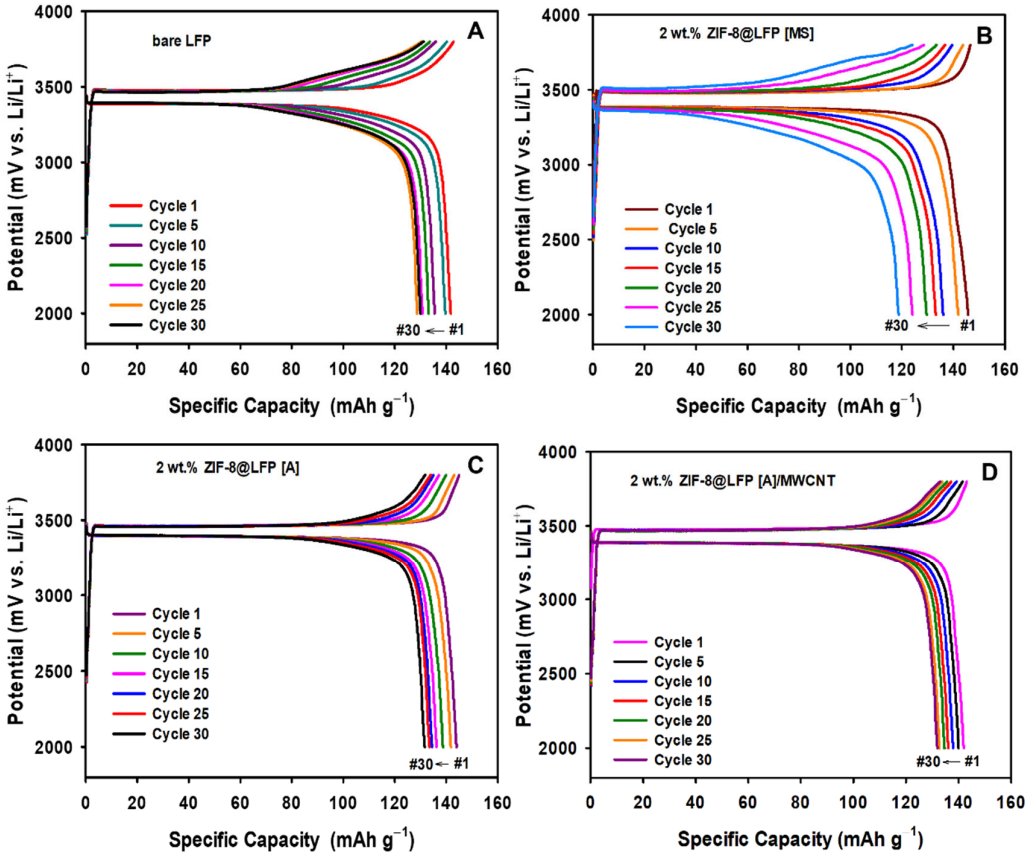

Figure S7. Charge-discharge curves of **(A)** bare LFP, **(B)** 2 wt.% ZIF-8@LFP [MS], **(C)** 2 wt.% ZIF-8@LFP [A] and **(D)** 2 wt.% ZIF-8@LFP [A]/MWCNT electrodes at 0.1C/0.1C rate for 30 cycles.

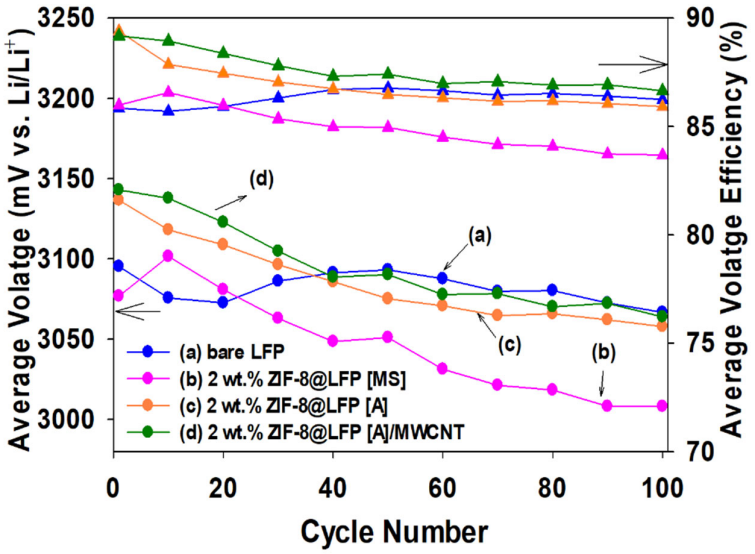

Figure S8. Average discharge voltage and voltage efficiency profile of the (a) bare LFP, (b) 2 wt.% ZIF-8@LFP [MS], (c) 2 wt.% ZIF-8@LFP [A], and (d) 2 wt.% ZIF-8@LFP [A]/MWCNT electrodes

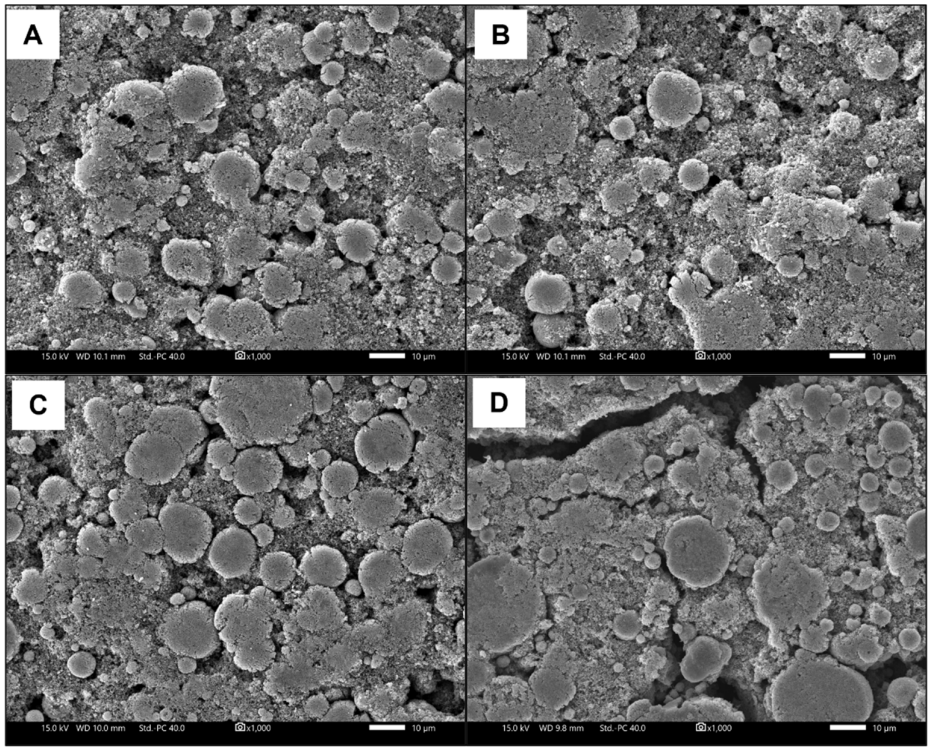

Figure S9. SEM images of 2 wt.% ZIF-8@LFP [A]/MWCNT electrode before **(A)** and after

(A) 100 cycles at 1C rate. SEM images of the bare LFP electrode before **(C)** and after **(D)** 100 cycles at 1C rate.

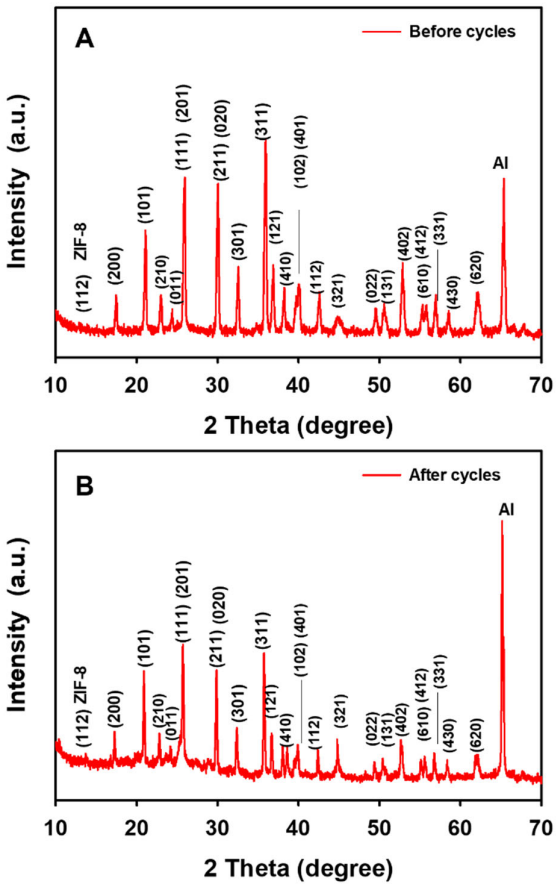

Figure S10. XRD patterns of 2 wt.% ZIF-8@LFP [A]/MWCNT electrode before **(A)** and after **(A)** 100 cycles at 1C rate.

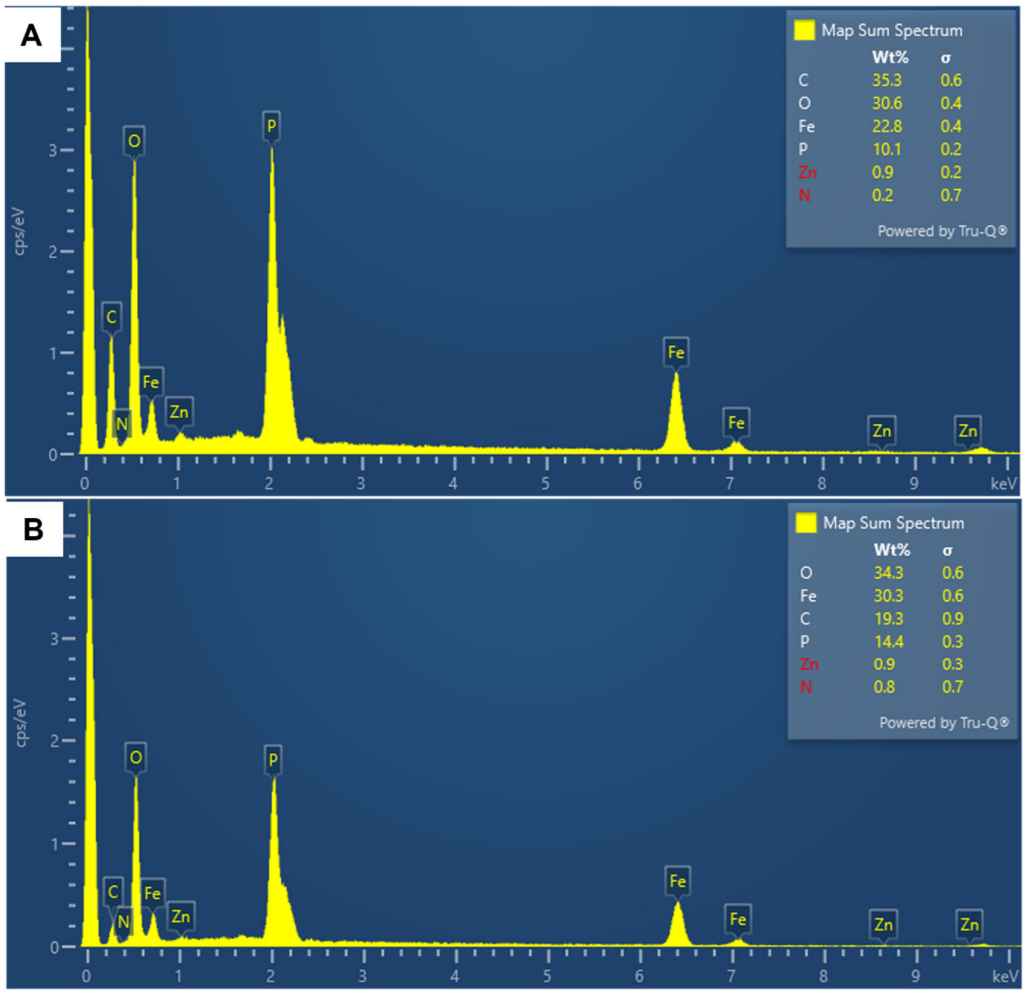

Figure S11. EDX analysis of 2 wt.% ZIF-8@LFP [A]/MWCNT electrode before **(A)** and after **(A)** 100 cycles at 1C rate.

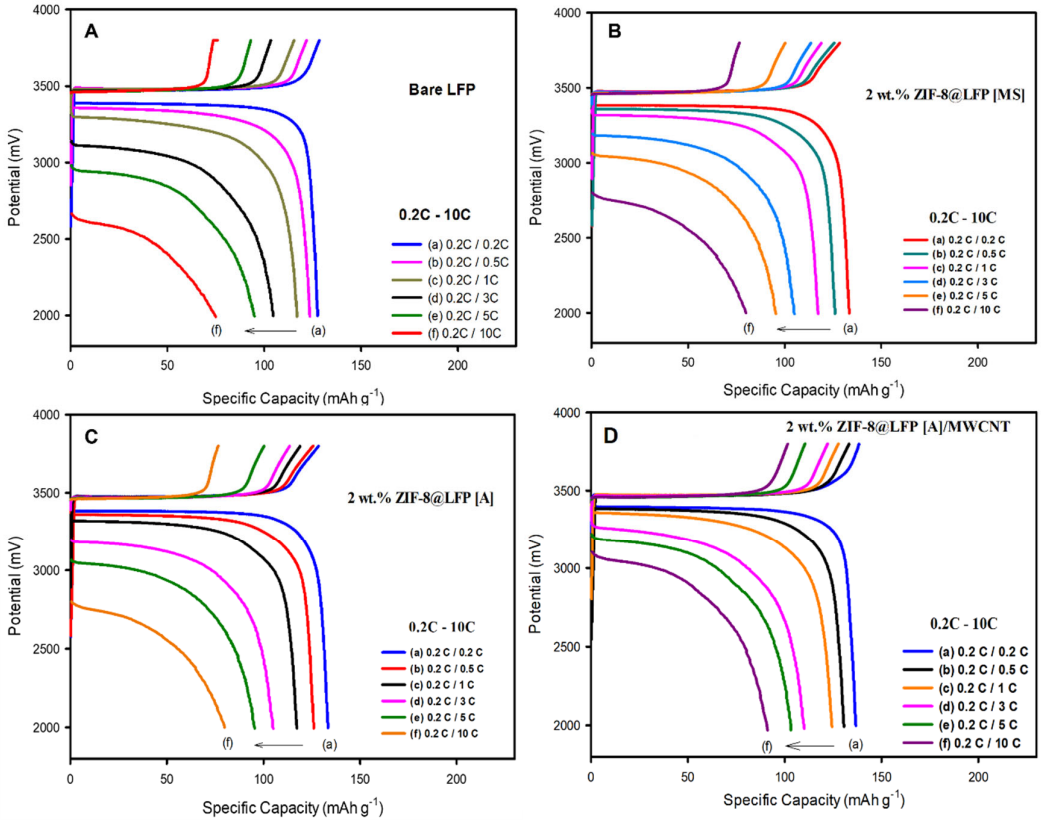

Figure S12. Charge-discharge curves of **(A)** bare LFP, **(B)** 2 wt.% ZIF-8@LFP [MS], **(C)** 2 wt.% ZIF-8@LFP [A] and **(D)** 2 wt.% ZIF-8@LFP [A]/MWCNT electrodes at 0.2 - 10C rates.

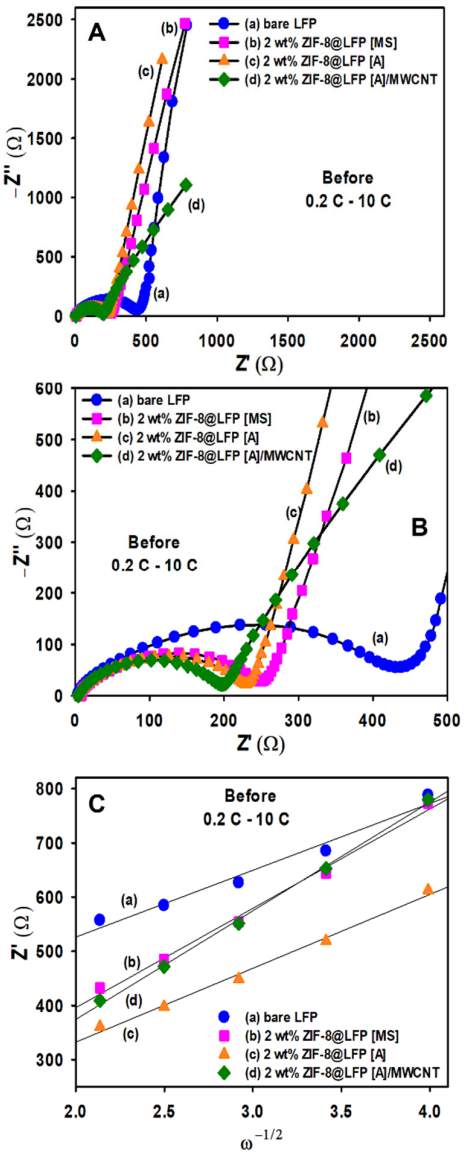

Figure S13. (A) Nyquist plots of the (a) bare LFP, (b) 2 wt.% ZIF-8@LFP [MS], (c) 2 wt.% ZIF-8@LFP [A] and (d) 2 wt.% ZIF-8@LFP [A]/MWCNT electrodes before high rate (at 0.2C - 10C) cycles. **(B)** The magnified view of Figure S7A. **(C)** The linear dependence of Z' versus $\omega^{-1/2}$ plot for before high rate (0.2C - 10C) cycles.